

**Design of a Restartable Clock Generator
for Use in GALS SoCs**

by Hu Wang, Bachelor of Science

A Thesis Submitted in Partial
Fulfillment of the Requirements
for the Master of Science Degree

Department of Electrical and Computer Engineering
in the Graduate School
Southern Illinois University Edwardsville
Edwardsville, Illinois

August 6, 2008

ABSTRACT

Design of a Restartable Clock Generator for Use in GALS SoCs

by

Hu Wang

Advisor: Dr. George L. Engel

This thesis presents the design of an instantaneously restartable crystal-controlled clock generator in a 90 nm CMOS (Complementary Metal-Oxide Semiconductor) twin-well process. The clock generator is a critical component in a newly proposed blended design methodology in which clocked subsystems are connected by using clockless sequencing networks. The novel design overcomes the problem of poor control of the clock period generally associated with pausable clocks.

The generator described herein is fully compatible with any deep-submicron technology and insensitive to process variations. The design uses only ‘regular’ threshold voltage FETs (Field Effect Transistors). Simulations indicate that the design is capable of functioning correctly at frequencies up to 1 GHz irrespective of process corner while operating from a single 1 Volt supply and consuming 10 mW of power. The duty cycle of the clock is near 50%, and the delay in restarting the clock is small, less than 1.5 periods.

ACKNOWLEDGEMENTS

I would like to thank Dr. George Engel for his support and guidance as well as the opportunity to participate in this research project without which I could not have progressed so far. I would also like to thank Jerry Cox, Senior Professor of Computer Science, Washington University, Saint Louis, for his advice during the various stages of this project. I would like to thank my fellow researchers, Dinesh Dasari, Nagendra Sai Valluru for their help.

I would like to acknowledge the contributions of Sasi K. Tallapragada. Mr. Tallapragada successfully designed, fabricated (in a TSMC 0.25 μm process), and tested an earlier version of the designed presented here. His work laid the groundwork for the design described in this thesis. I also wish to thank the National Science Foundation and Blendics, LLC. This work has been supported by a NSF-STTR grant from the Blendics company.

I would like to thank Dr. Scott Umbaugh, Dr. Scott Smith, and Dr. Brad Noble, ECE faculty members at SIUE, who actively encouraged me. With their support, I was able to explore new areas. I would also like to thank Dr. Bob Leander and the rest of the ECE faculty who also have supported me throughout my education at SIUE.

Finally, I wish to thank my family for being patient with me and encouraging me throughout the entire of my college experience. In particular, I would like to thank my wife Yue Cheng, without whom I may not have finished.

TABLE OF CONTENTS

ABSTRACT	ii
ACKNOWLEDGEMENTS	iii
LIST OF FIGURES	vi
LIST OF TABLES	vii
Chapter	
1. INTRODUCTION	1
Background	1
Blended Design Methodology	2
Objective and Scope of Thesis	6
2. CLOCK GENERATOR DESIGN	7
Overview of the Clock Generator	7
Principle of Operation	8
Initial Analog Multiplier Design	9
Improved Analog Multiplier Design	15
High-Speed Comparator Design	18
SR Latch and OR Gate Design	19
Track and Hold Circuit Design	20
3. NON-IDEAL EFFECTS	22
Channel Length Modulation	22
Sensitivity Analysis	23
Mismatch and Offset Analysis	26
Device Sizing	28
4. SIMULATION RESULTS	32
Analog Multiplier Simulation	32
Frequency Response of Symmetric Miller OTA	32
Hold Signal Verification	34
Track and Hold Circuit Simulation	35
Restartable Clock Generator Simulation	36

5. CONCLUSIONS AND FUTURE WORK.....	39
Conclusions.....	39
Future Work.....	40
REFERENCES	41

LIST OF FIGURES

Figure		Page
1.1	Data processing subsystem with a control wrapper and clock generator	4
1.2	Pair of processing elements communicating using clockless sequencing network .	5
2.1	Architecture of restartable clock generator.....	7
2.2	Initial analog multiplier.....	10
2.3	Original combiner circuit [Hsi:98].....	14
2.4	Improved combiner circuit.....	15
2.5	Automatic gain control circuit for resistive PFET	16
2.6	Symmetric Miller OTA.....	17
2.7	High-speed analog comparator	18
2.8	SR latch circuit.....	19
2.9	Track and hold circuit	20
4.1	Analog multiplier simulation	33
4.2	Frequency response of symmetric Miller OTA	33
4.3	Hold signal verification.....	34
4.4	Transient response of T/H circuit	35
4.5	Frequency response of T/H circuit.....	36
4.6	Clock generator simulation.....	37
4.7	Delay associated with restarting the clock.....	38

LIST OF TABLES

Table		Page
3.1	Comparison of simulation results	23
3.2	Simulation results of parameter values across process corners	25
3.3	Estimated and simulated results in initial and improved multipliers.....	25
3.4	Combiner FET sizes.....	28
3.5	Bias circuit and OTA FET sizes	30
3.6	NAND gate and T/H circuit FET sizes	30
3.7	Comparator FET sizes.....	31

Chapter 1

INTRODUCTION

Background

Currently, verification occupies 60% to 80% of the engineering hours expended on the design of complex integrated circuits (ICs). Unless there is a significant paradigm shift, the engineering effort directed toward verification is sure to continue to grow as chip density grows. Module reuse along with elimination of the global verification component of chip design has the potential to cut the design time of future chips by up to an order of magnitude. This can be accomplished by reusing previously verified modules and by connecting these modules with provably-correct, delay-insensitive pathways. As a result, all global verification will be process independent, and only local verification will be process specific. These technology advantages can curtail the explosive time-to-market growth of future ICs as Moore's law drives chip transistor density ever upward.

We are developing such a methodology, one that blends clockless and clocked systems and eliminates the need for global verification. The methodology utilizes a clockless sequencing and communication network interconnecting locally verifiable clocked modules so that all global signaling exhibits correct behavior, independent of the specific IC process used for implementation.

Delay-insensitive control and data paths are composed from a set of six control elements implemented as standard cells and designed to be completely free of both combinational and metastability hazards. This guarantee is valid, provided the composition of elements follows a few simple rules. Fan-in and fan-out are possible for both control and

data paths, and there is no requirement for global control mechanisms. Furthermore, sending data in packets of arbitrary length (including a single byte or word) is supported.

If the local domain is clocked, the use of a synchronizer between the local and global domains is avoided by means of a novel clock generator [Cox:88], [Cox:07]; the design of which is the focus of this thesis. The clock generator can function with a remote crystal source or with a local, MEMS-based, all-silicon source and can pause and then resume asynchronously, in either case. Hazards due to poor synchronizer design are avoided.

Adding the clock generator to a clocked subsystem makes it appear to the rest of the system as if it were clockless, *i.e.*, operating completely asynchronously. These clocked subsystems may then be composed with the rest of the system's components, utilizing asynchronous control and data paths. As a consequence, even for clocked subsystems, the need for verification of global timing is avoided by use of global paths that function with complete insensitivity to variations in delay.

This methodology for blending of clockless and clocked systems is a special case of the Globally Asynchronous, Locally Synchronous (GALS) [Cha:73] design approach. The special features of our approach are the guaranteed correctness of the compositions of the control elements and freedom from all combinational and metastability hazards.

Blended Design Methodology

GALS systems suffer from either poor control of the local clock period or the potential for synchronizer failure. Synchronizer failures occur when setup and hold time constraints are violated in a system consisting of flip-flops or registers. Chapiro [Cha:73] proposed a taxonomy for GALS circuits based on the method used for synchronizing data with the local clocks. The methodology presented within this thesis falls into his

“escapement” category [Tra:91]. It avoids the problem of synchronizer failures by stopping the clock and then restarting it when data is valid. In the majority of similar schemes presented in the literature, the pausable clock is implemented using a delay-based circuit or ring oscillator. Pausible clocks are often discussed in the relevant literature; for example, in [Tra:91], [Dob:99], [Ami:07], [Yun:99], [Gür:06], and [Bei:08].

In the scheme proposed in this research, the clock generator is based on a stable crystal oscillator, yet *functions* like a delay-based clock. We call it a “restartable” clock to distinguish it from existing pausable clocks. Unlike a conventional crystal oscillator, it can be started at any instant in time, taking on a phase reference determined by that starting instant. Two (or more) processing elements with such clocks can carry out the transfer of data without the requirement for synchronization and can thus be free of any synchronizer failure.

This freedom from synchronizer failure is accomplished by an asynchronous layer between the two subsystems such that the two systems are no longer completely independent. The purpose of this asynchronous layer is to initiate the operation of the data processing subsystem’s local clock, and to signal an acknowledgment of the completion of that action. Because none of the subsystem clocks are fixed in their phase, the blended design methodology will never produce a system that is capable of a synchronizer failure. This is true even though their periods are controlled by a crystal oscillator. When arbitration is required in the asynchronous layer, an arbiter control element waits until circuit resolution is complete before proceeding and thereby avoids metastability errors. Fig. 1 illustrates a data processing subsystem embedded in a control wrapper along with the clock generator.

The clock generator serves as a local clock to the data processing subsystem. The heavy solid lines indicate data paths between different data processing subsystems and lighter lines indicate sequencing paths between control elements indicated by circles. The purpose of

the control wrapper is to initiate the data processing subsystem's local clock and to signal an acknowledgement indicating that the action is completed.

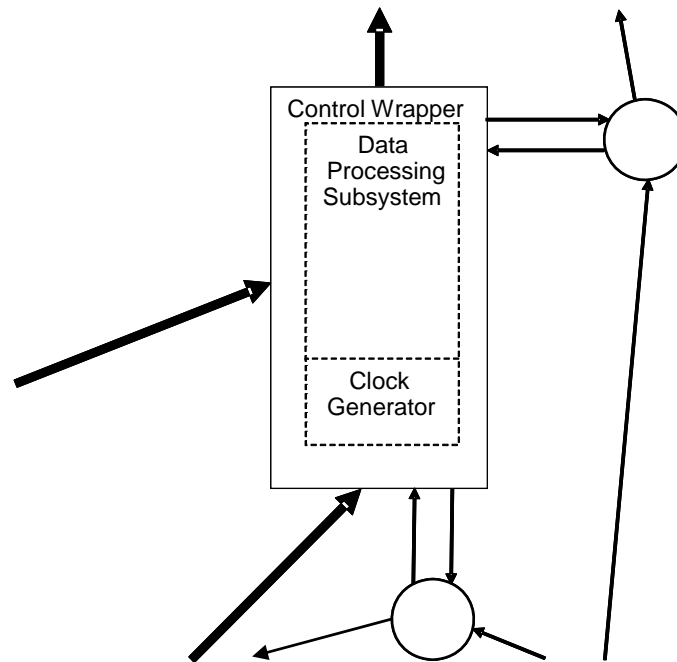


Fig. 1.1 Data processing subsystem with a control wrapper and clock generator

The control wrapper in Fig. 1.1 is designed by using control elements similar to those that were defined by Clark *et. al.* in 1967 [Cla:67]. The control elements are the *Fork*, *Merge*, *Join*, *Dual-Join*, and *Arbiter*. A sixth control element, the *Transfer*, has also been recently defined (although it was implicit in the earlier work). This element transfers control signals between the global clockless domain and a local domain with timing constraints.

All six control modules have been simulated and behave as predicted. Many complex systems were built utilizing an equivalent set of control elements [Cla:74], an indication of their great expressive power. These elements were all externally delay-insensitive (DI) allowing the composition of endlessly scalable systems.

An example application of our blended methodology is illustrated in Fig. 1.2. Two processing elements (A and B) communicate using a clockless sequencing network. The

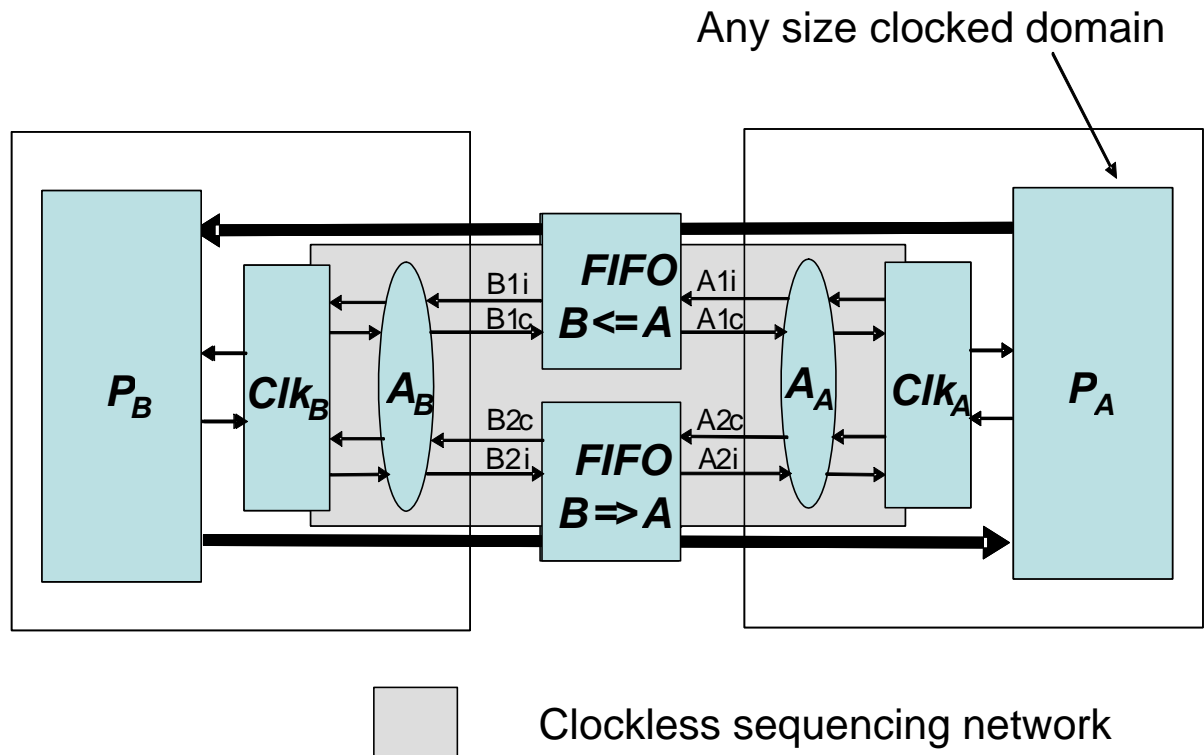


Fig. 1.2 Pair of processing elements communicating using clockless sequencing network

forementioned initiation and completion signals are explicitly depicted in the figure. The block indicated as ‘ A ’ is an Arbiter and the block indicated as ‘ Clk ’ is the “restartable” clock.

These control elements can provide a high-level abstraction for designing complex asynchronous SoCs (Systems on Chips), but they must be brought up to date with today’s technology by avoiding any dependence on IC process characteristics and by becoming internally, as well as externally delay insensitive. Toward this end, Petri net models of the six elements and their environments have been defined [Cox:05] and their reachability graphs calculated. The ternary test [Ung:69] for instability and metastability hazards can be applied

to verify the absence of the former and provide the necessary information for control of the latter. Systems composed from the resulting element set are delay-insensitive and hazard-free, independent of the IC process in which the elements are implemented.

Objective and Scope of Thesis

The objective of this thesis work was to design an instantaneously restartable crystal controlled clock generator in a IBM 90nm CMOS twin-well process. As a critical component in a newly proposed blended design methodology, it can be used in GALS SoCs.

There are five chapters in this thesis. In Chapter 2, the design of the restartable clock generator is described in detail. Non-ideal effects including channel length modulation, offset due to mismatches and an analysis of the sensitivity of the design to variations in IC process parameters are discussed in Chapter 3. Transistor sizes for the circuits used in the various sub-systems described in Chapter 2 are also given in Chapter 3. Chapter 4 presents the simulation results for the clock generator. Finally, conclusions and future work are presented in Chapter 5.

CHAPTER 2

CLOCK GENERATOR DESIGN

Overview of the Clock Generator

The clock generator is based on a stable crystal oscillator, yet functions like a delay-based clock generator. Unlike a crystal oscillator, the proposed clock generator can be started or stopped at any instant of time by taking on a phase reference determined by the starting instant. The architecture of the clock generator is illustrated in Fig. 2.1.

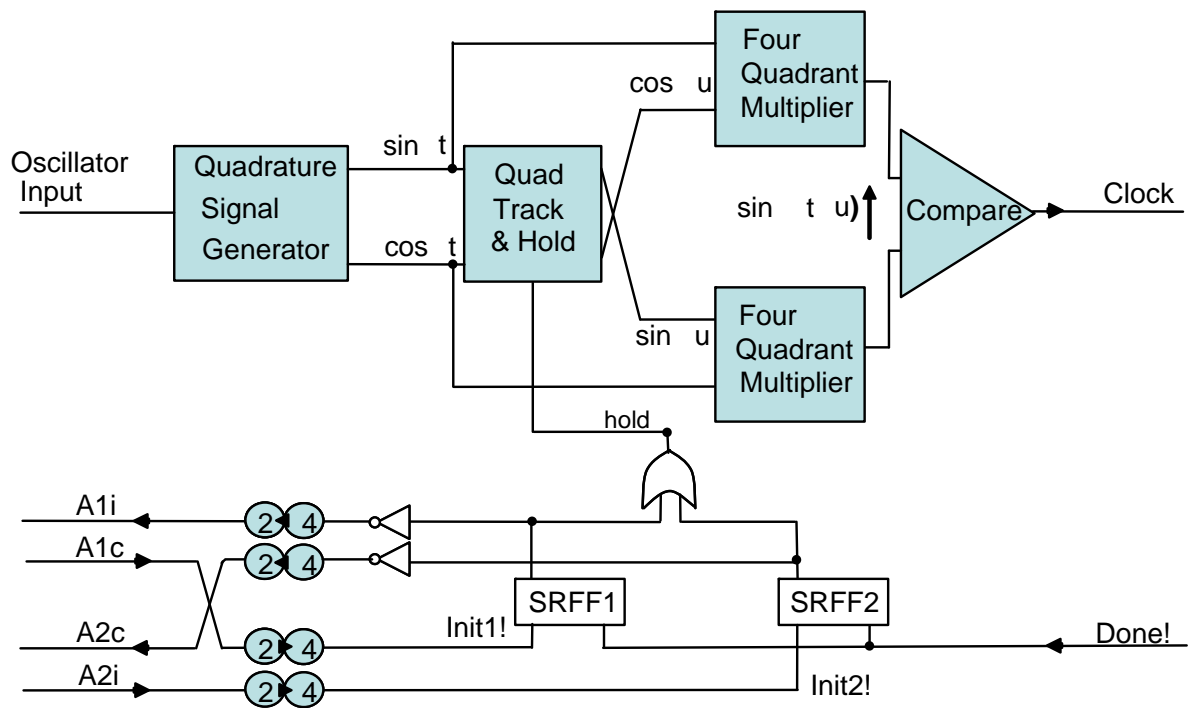


Fig. 2.1 Architecture of restartable clock generator

The ‘!’ suffix on signal names indicates four-phase signaling which means that the signal must return to its previous level (*i.e.* a pulse). Information is transmitted via transitions for two-phase signaling. The act of “starting” the clock is accomplished when either one of the ‘*Init!*’ signals is asserted. After the data processing completes, the subsystem activates the ‘*Done!*’ signal, which stops the clock. Data communication between the subsystems can then commence.

Principle of Operation

The clock generator, depicted in Fig. 2.1, is constructed from the following: a pair of fully-differential analog multipliers, a current-mode comparator, a quad track-and-hold (*T/H*) circuit, a pair of *SR* latches, and an *OR* gate. The quadrature signals are generated from a crystal or MEMS-based oscillator [Mob]. The design of the circuit used to generate these quadrature signals is outside the scope of this thesis and will not be discussed further.

The operation of the clock generator is based on the simple trigonometric identity [Cox:88] and [Cox:07] given by

$$\sin \omega(t - u) = \sin \omega t \cdot \cos \omega u - \cos \omega t \cdot \sin \omega u \quad (2.1)$$

where, ‘ ω ’ is the angular frequency in *rad/sec*, ‘ t ’ is time in seconds and ‘ u ’ is the delay in seconds introduced with respect to the start of the clock generator *i.e.* the assertion of one of the ‘*Init!*’ signals.

The clock is generated when either one of two ‘*Init!*’ signals is asserted. Then, the output of one of the *SR* latches which initially are both reset is set. The high level on the hold input of the *T/H* circuits forces them into the “hold” phase. If the ‘*Done!*’ signal is asserted, it resets both *SR* latches. This places the *T/H* circuits into the “track” mode.

The outputs of the track and hold circuits shown in Fig. 2.1 correspond to the state of the clock generator during the hold phase *i.e.* when the clock is running. In reality all eight inputs to the analog multipliers pass through *T/H* circuits. The additional *T/H* circuits (on the $\pm \sin\omega t$ and $\pm \cos\omega t$ inputs) are always held in the “track” mode and were inserted to equalize the delays so that all signals arrive at their respective inputs to the analog multipliers at the same time.

The *T/H* circuit was implemented using a simple CMOS transmission gate with the input capacitance of the multiplier serving as the sampling capacitor. The analog comparator compares the differential input signal, producing a clock signal which is high when this signal is positive and low when it is negative.

When *T/H* circuits in Fig. 2.1 are placed into track mode, the clock is to be stopped. During this circumstance, the analog inputs to the upper multiplier and the lower multiplier in Fig. 2.1 are identical, thereby, presenting a zero differential signal to the comparator. A small systematic offset must exist or must be inserted into the comparator to ensure that the comparator output is driven low (and remains low) when the differential signal is zero.

In the clock generator design, the analog multiplier is the most prominent component. The analog multiplier is used to implement the product of two sinusoidal inputs. As shown in the equation (2.1), two multipliers are required. The following section will explore the design of the analog multiplier in more detail.

Initial Analog Multiplier Design

In this section we discuss our initial [Tal:05] four quadrant analog multiplier design which is based on a circuit first presented by Hsiao *et. al.* [Hsi:98]. In following section, we demonstrate how the design may be modified to reduce the sensitivity of the circuit to

The differential nature of the circuit is the central feature which allows high performance, even when using this very simple structure to implement the multiplier.

A single combiner, shown in Fig. 2.3, consists of two NMOS transistors operating in the saturation region and a resistor, R .

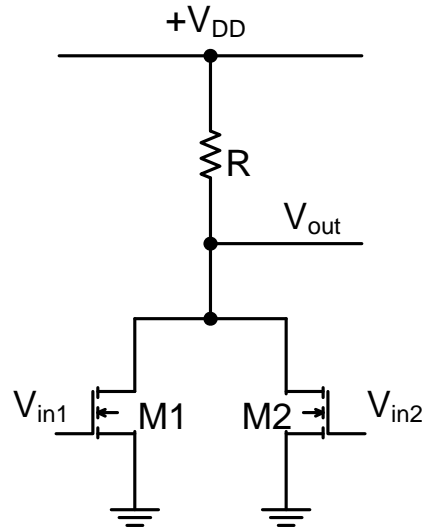


Fig. 2.3 Original combiner circuit from [Hsi:98]

The combiners in the multiplier are divided into two stages. We refer to the combiners labeled as 1, 2, 3, and 4 in Fig. 2.2 as “first-stage” combiners. The “second-stage” combiners (labeled 5 and 6) are a pair of NMOS transistors working in the saturation region with the resistor R omitted. The purpose of the resistor in the second-stage combiner of [His:98] was to transform the output current into an output voltage. As indicated in the equation (2.1), the differential outputs from the analog multipliers must be subtracted in order to produce the delayed sinusoid. The taking of this difference is more easily performed in the current domain, and so we allow our multiplier to have a current rather than a voltage output.

The transistors in the analog multiplier from [Hsi:98] are operated in saturation, and the current in each combiner can be represented by the square law characteristic of a MOS transistor given by

$$i_{DS} = \frac{1}{2n} \cdot K_{pn} \cdot S_n \cdot (v_{GS} - V_{TN})^2 \quad (2.3)$$

where i_{DS} is the drain-to-source current of the NMOS transistor, v_{GS} is the gate-to-source voltage, V_{TN} is threshold voltage, K_{pn} is transconductance parameter, n is the subthreshold slope factor, and S_n is the shape factor (W_n / L_n where W_n is the width and L_n is the length of the NFET). We assume, for simplicity, that all of the NFETs in the multiplier are matched and we ignore second-order effects such as channel length modulation.

The output node voltage v_a of the first combiner shown in Fig. 2.3 is given by

$$v_a = V_{DD} - i_a \cdot R \quad (2.4)$$

where R is resistance, V_{DD} is the supply voltage, and i_a is the sum of the drain-to-source currents for transistors M_1 and M_2 of the first combiner. The current flowing in each transistor is given by the expression in equation (2.3).

Substituting the input voltages $V_B + v_1$ and $V_B + v_2$ which are applied as gate voltages to the transistors M_1 and M_2 respectively and using equation (2.3), then the expression of v_a in equation (2.4) can be written as

$$v_a = \frac{-R}{2n} \cdot K_{pn} \cdot S_n (V_B + v_1 - V_{TN})^2 + \frac{-R}{2n} \cdot K_{pn} \cdot S_n (V_B + v_2 - V_{TN})^2 + V_{DD} \quad (2.5)$$

Expanding the above expression and collecting like terms, one finds

$$v_a = V_{DD} - \frac{S_n \cdot K_{pn} \cdot R}{2n} \cdot v_1^2 - \frac{S_n \cdot K_{pn} \cdot R}{2n} \cdot v_2^2 - \frac{S_n \cdot K_{pn} \cdot R \cdot (V_B - V_{TN})}{n} \cdot v_1 - \frac{S_n \cdot K_{pn} \cdot R \cdot (V_B - V_{TN})}{n} \cdot v_2 - \frac{S_n \cdot K_{pn} \cdot R \cdot (V_B - V_{TN})^2}{n} \quad (2.6)$$

Similarly, the output node voltages v_b through v_d for combiners 2 through 4 also have the same expression shown in equation (2.6) except that the sign of the terms containing v_1 and v_2 change based on the phase of the signal that is applied to the corresponding combiner as shown in Fig. 2.2. The expressions for the multiplier output currents i_{op} and i_{om} are then

$$i_{op} = \frac{S_n \cdot K_{pn}}{2n} [v_a^2 + v_b^2 - 2V_{TN} \cdot (v_a + v_b) + 2V_{TN}^2] \quad (2.7a)$$

$$i_{om} = \frac{S_n \cdot K_{pn}}{2n} [v_c^2 + v_d^2 - 2V_{TN} \cdot (v_c + v_d) + 2V_{TN}^2] \quad (2.7b)$$

The differential output current of the analog multiplier i_{out} is thus obtained by subtracting (2.7b) from (2.7a), and after some algebraic manipulation one obtains the following expression

$$i_{out} = K_{mult} \cdot v_1 \cdot v_2 \quad (2.8)$$

$$\text{where } K_{mult} = 4 \left[\left(\frac{S_n \cdot K_{pn}}{n} \right)^3 \cdot R^2 \cdot (V_B - V_{TN})^2 \right]$$

The multiplier gain constant, K_{mult} , is strongly dependent on process parameters. The value of K_{pn} changes by tens of percent from one process corner to another as does the sheet resistance of the material used to implement the resistance, R . Moreover, both of these parameters display significant temperature dependence.

The expression in equation (2.8) for K_{mult} may be re-written as follows

$$K_{mult} = \left[\frac{2V_R}{(V_B - V_{TN})} \right]^2 \left(\frac{S_n \cdot K_{pn}}{n} \right) \quad (2.9)$$

where V_R is the DC voltage drop across the resistor, R . Equation (2.3) was used to compute the quiescent current through the resistor. We observe in equation (2.9) that the first term is associated with the “first-stage” combiners shown in Fig. 2.2, while the second term is due to the “second-stage” combiners. Little can be done to remove the variation in the multiplier gain constant due to parameters associated with the second-stage combiners, but it is possible to remove much of the process dependence associated with the “first-stage” combiners. In the following section, we propose a modification to the combiner circuit in Fig. 2.3 which addresses this issue.

Improved Analog Multiplier Design

As demonstrated in the previous section, the gain of the multiplier depends strongly on the DC voltage across the resistor. Unfortunately, this voltage is highly sensitive to process variations. If this voltage could be made independent of process, the gain of the multiplier, K_{mult} would be less dependent on process corner.

In order to reduce the sensitivity of K_{mult} to variations in processes and to yield a design that is free of resistors, the resistor used in the “first-stage” combiner was replaced with a PMOS transistor, M_3 , operating in the resistive region. Also, use of a PFET to realize the resistor, R , saves area. The modified “first-stage” combiner is shown in Fig. 2.4.

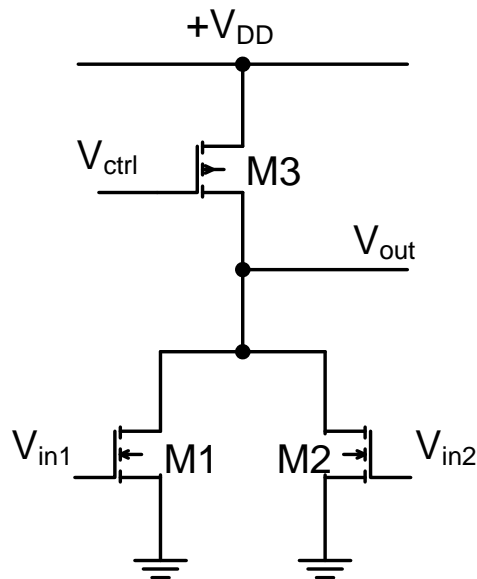


Fig. 2.4 Improved combiner circuit

For a PFET biased in the resistive region [All:03], R_{eq} can be calculated as follows

$$R_{eq} = \frac{n}{K_{pp} \cdot S_p \cdot (V_{DD} - V_{ctrl} - |V_{TP}|)} \quad (2.10)$$

where V_{ctrl} is the gate control voltage, V_{TP} is the threshold voltage of the PFET, K_{pp} is the transconductance parameter of the PFET, and S_p is the shape factor. While in general there are linearity concerns when FETS are used to simulate resistances, those concerns are mitigated here by the fact that the analog multiplier design of Fig. 2.2 is fully differential and because intermediate levels of distortion do little to interfere with the ability of the comparator in Fig. 2.1 to discriminate zero crossings. By adjusting the control voltage, V_{ctrl} , the resistance can be altered and in turn the DC voltage across device M_3 tuned to the desired value (*i.e.* the value which produces the desired K_{mult}).

In order to make this “tuning” automatic, an **additional** combiner was added to the design as illustrated in Fig. 2.5.

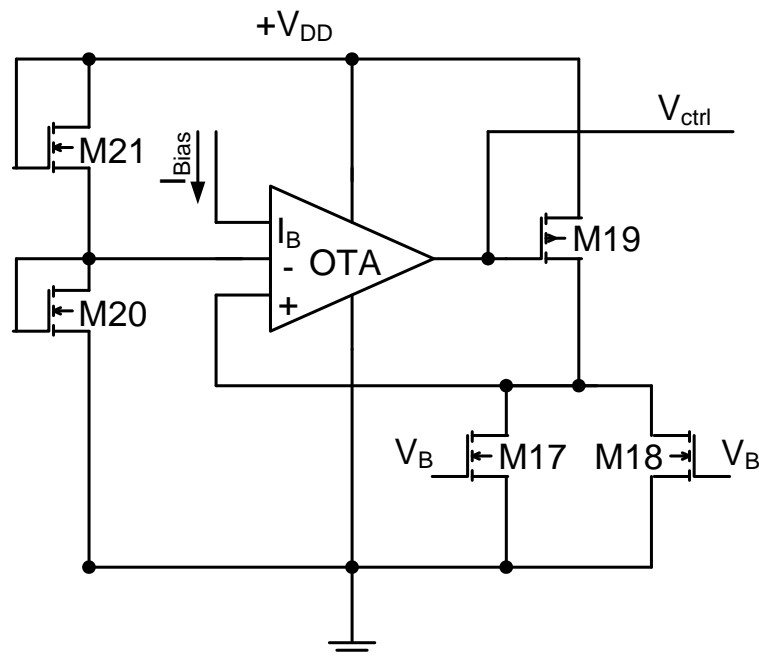


Fig.2.5 Automatic gain control circuit for resistive PFET

Transistors M_{17} and M_{18} are the same size as the NFETS (M_1 and M_2) used in the combiner circuit from Fig. 2.4. M_{19} matches PFET M_3 . The OTA (Operational Transconductance Amplifier) is of the symmetric Miller type [Lak:94]. Devices M_{20} and M_{21} are matched. They implement a voltage divider. The voltage on the inverting input is half of the supply voltage. As a result of negative feedback, the OTA adjusts its output until the voltage at the non-inverting input is also $V_{DD}/2$. The voltage, V_{ctrl} , on the gate of M_{19} is then distributed to the gates of the resistive PMOS devices in *both* analog multipliers depicted in Fig. 2.1.

For simplicity and considering of the limitations resulting from the use of a 1 Volt power supply, we chose a symmetric Miller OTA design. The circuit schematic is given in Fig.2.6.

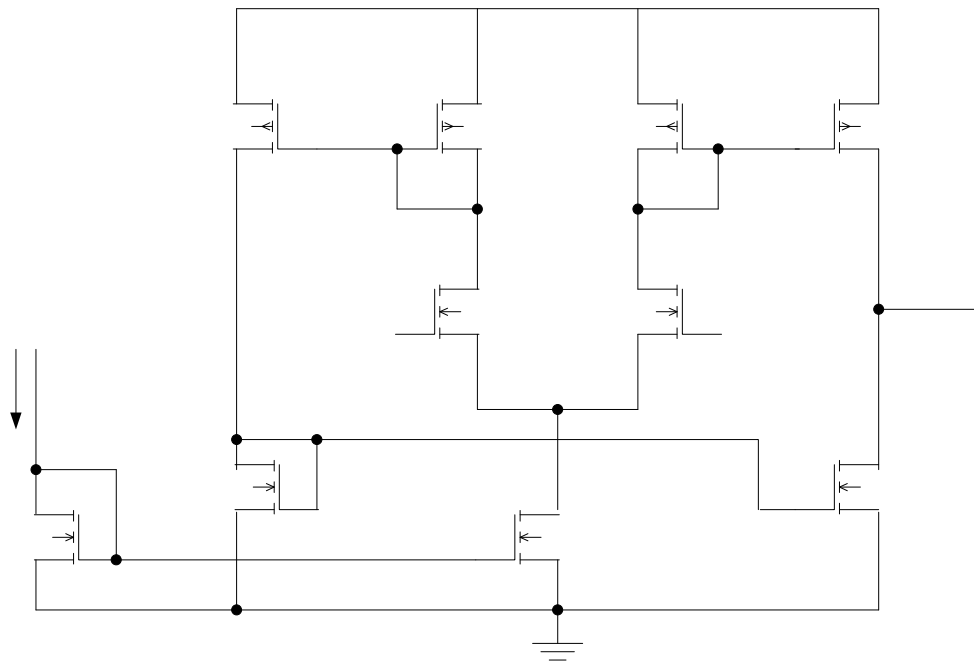


Fig.2.6 Symmetric Miller OTA

A differential pair is formed by the matched input transistors, M_1 and M_2 . M_3 and M_4 are load devices, matched as well, each of which constructs a current mirror with their counterpart devices M_5 and M_6 . The output current of transistor M_5 is then mirrored once again by the current mirror formed using devices M_7 and M_8 . Finally, the output voltage, V_{out} is sum of the small-signal currents in M_6 and M_8 multiplied by the parallel combination of the small-signal output resistances r_{o6} and r_{o8} . All current levels are determined by the bias current I_{BIAS} , which is $10\mu\text{A}$.

High-Speed Comparator Design

The high-speed comparator (adapted from [All:03]) illustrated in Fig. 2.7 is used to convert the differential sinusoidal current output from the multipliers into a square-wave clock output. Transistor pair M_5 - M_6 form a current mirror as do transistors M_7 - M_8 . The cross-coupled transistors M_2 - M_3 implement a high-speed NMOS latch. Diode-connected transistors M_1 and M_4 provide hysteresis and help to establish the common-mode input voltage for the

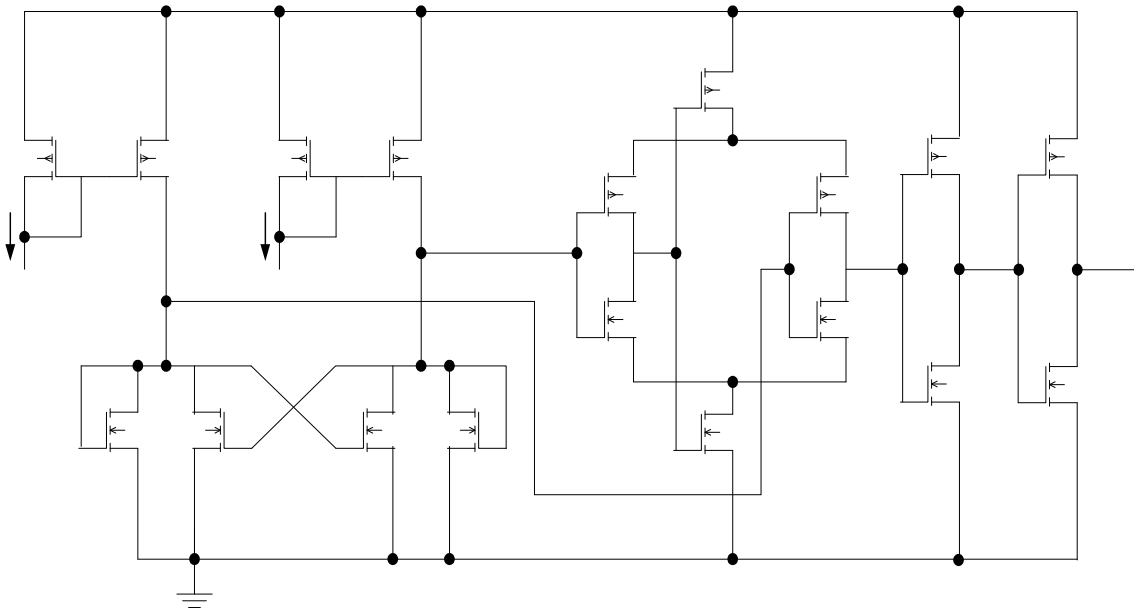


Fig. 2.7 High-speed analog comparator

self-biased differential amplifier formed by devices M_9 through M_{14} . The output of the self-biased differential amplifier drives a pair of cascaded push-pull output drivers comprised of FETS M_{15} - M_{18} to guarantee a rail-to-rail clock output.

SR Latch and OR Gate Design

The *SR* latch in Fig. 2.1 is constructed by two cross-coupled *NAND* gates. The *NAND* gate is implemented using a fully complementary logic structure. Since the inputs of the *OR* gate can be set to active low by means of connecting them to the inverting outputs (Q_{bar}) of the *SR* latches the *OR* gate is simply replaced by a *NAND* gate. Using only *NAND* gates simplifies the layout of the clock generator. Fig. 2.8 illustrates the *SR* latch and the *NAND* gate used in the design of the latch.

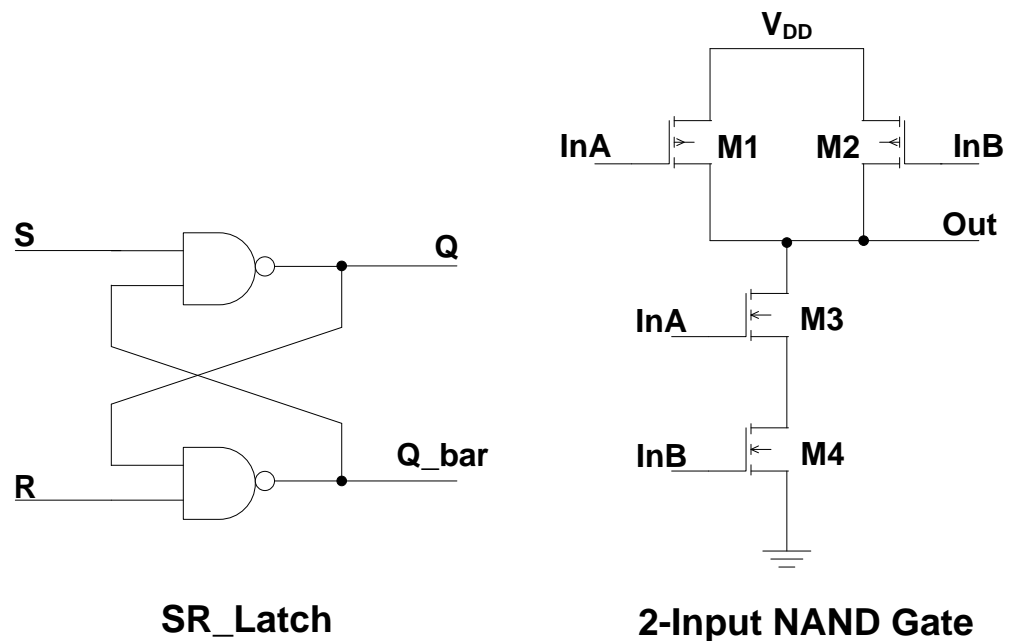


Fig. 2.8 *SR* latch circuit

The function of the *SR* latches is to latch the ‘*Init!*’ or ‘*Done!*’ signals. Whenever the active low ‘*Done!*’ signal is applied to the ‘*R*’ input nodes of the *SR* latch it resets the latch. The ‘*hold*’ signal (See Fig. 2.1) will stop the clock output. In the same way, the clock output will restart if either of the ‘*Init!*’ signals that are tied to the ‘*S*’ input node of the *SR* latch pulses low.

Track and Hold Circuit Design

The track and hold circuit (*T/H*) is composed of a simple CMOS transmission gate with the input capacitance of the analog multiplier input serving as the tracking capacitor. Two cascaded inverters are used to supply the switching signals for the transmission gate. The *T/H* circuit schematic is illustrated in Fig. 2.9.

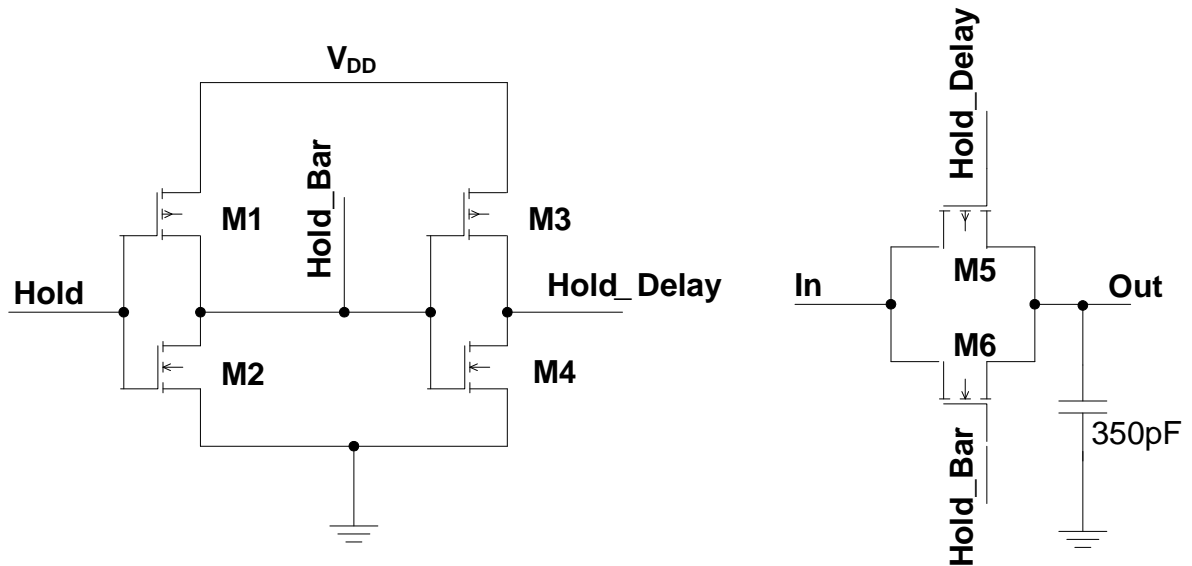


Fig. 2.9 Track and hold circuit

The T/H circuit will be set into the “Track” mode as long as the ‘Hold’ signal is low. During this time the input sinusoidal signal can pass through the transmission gate (delayed by a small amount in time). Whenever the ‘hold’ signal transitions from low to high, the T/H circuit goes to the “Hold” mode that will result in the output of the transmission gate retaining the analog value present at the input to of the T/H a short time before the ‘Hold’ signal went high .

CHAPTER 3

NON-IDEAL EFFECTS

In this chapter, we consider effects which lead to the multiplier displaying non-ideal behavior. First, we look at the effect of channel length modulation upon multiplier performance. We then investigate the effect of process parameter variations on expected performance by performing a sensitivity analysis. We finally consider how mismatch and offset affect the overall performance of the clock generator. Since the results of the offset analysis played a significant role in determining the final transistor sizes, we conclude the chapter with information regarding the size of the devices eventually selected.

Channel Length Modulation

The I - V characteristic of a FET given in equation (2.3) is ideal and does not account for the effects of channel length modulation. As drain voltage increases (in excess of the saturation voltage), the effective channel length of a FET decreases resulting in an increase in current [All:03]. This effect can be accounted for in equation (2.3) with the addition of the factor $(1 + \lambda v_{DS})$ where v_{DS} is the drain-to-source voltage and λ is the channel length modulation factor (inversely proportional to the length of the device, L).

When the effects of channel length modulation are included, the expression for the multiplier gain, K_{mult} , in equation (2.9) changes slightly. The expression becomes

$$K_{mult} = \left[\frac{2V_R}{(V_B - V_{TN})[1 + \lambda \cdot (V_{DD} - V_R)]} \right]^2 \left(\frac{S_n \cdot K_{pn}}{n} \right) \quad (3.1)$$

In Table 3.1 we compare results for the analog multiplier obtained using the equations derived in this thesis and computed using MathCAD® with those obtained through electrical simulation using Cadence's *Spectre*® simulator. One observes that if λ is included, then the analytical predictions agree closely (within 5%) with the results obtained from electrical simulations.

I_{Req} is the DC drain-to-source current of PFET M_3 in the multiplier's first-stage combiners, V_{BO1} is the DC output voltage for the first-stage combiners, and I_{out} is the peak-to-peak differential current transferred to the NMOS latch in the comparator. For these simulations V_B was 570 mV, and the peak-peak amplitude of the quadrature inputs was 400 mV. The value for V_R was $V_{DD}/2$ i.e. 0.5 Volts.

TABLE 3.1

Comparison of simulation results

		Mathcad		Electrical Simulation
		With λ	Without λ	
Output of the multiplier's first-stage combiner	I_{Req}	680 μ A	604 μ A	706 μ A
	V_{BO1}	0.5 V	0.5 V	0.49 V
Peak-to-peak output	I_{out}	1.49 mA	1.59 mA	1.53 mA

Sensitivity Analysis

Since the multiplier gain constant, K_{mult} , is strongly dependent on process parameters (See equation 2.8 and 2.9), the current output of the multiplier varied from the nominal value as simulations were run at different process corners. In Chapter 2 an improved analog multiplier design was introduced which made the design (we claimed) less sensitive to process corner. In this section of the thesis we explore this claim in a quantitative way and

compare the performance of the “improved” multiplier with the “initial” design by using the method of sensitivity analysis.

In equation (2.8) the threshold voltage, V_{TN} , the transconductance parameter, K_{pn} , and the resistance, R , are subject to process variations. They change across process corners and result in the multiplier’s output current deviating from the nominal value. Using a sensitivity analysis we can easily obtain the fractional or relative gain variation, $\Delta K_{mult} / K_{mult}$ given by

$$\frac{\Delta I_{out}}{I_{out}} = \frac{\Delta K_{mult}}{K_{mult}} = 2 \cdot \frac{\Delta R}{R} + 3 \cdot \frac{\Delta K_{pn}}{K_{pn}} - 2 \cdot \frac{V_{TN}}{V_B - V_{TN}} \cdot \frac{\Delta V_{TN}}{V_{TN}} \quad (3.2)$$

where the expression of each Δ term represents the parameter’s variation. For example, ΔR , represents the difference between the value, R_{sim} simulated in a specific process corner and the typical value, R_{typ} . Resistor, R is implemented using N+ diffusion.

For the improved analog multiplier, similarly the relative gain variation is shown below but there is no $\Delta R/R$ term since the real resistor is replaced by a resistive PFET, and V_R is treated as constant due to the existence of the bias circuit.

$$\frac{\Delta I_{out}}{I_{out}} = \frac{\Delta K_{mult}}{K_{mult}} = \frac{\Delta K_{pn}}{K_{pn}} + \frac{2 \cdot V_{TN}}{V_B - V_{TN}} \cdot \frac{\Delta V_{TN}}{V_{TN}} \quad (3.3)$$

Table 3.2 indicates the absolute value and relative variation of each process parameter across different corners. The expected values of these variations were obtained through a series of simulations. The measurement of the threshold voltage V_{TN} and transconductance K_{pn} was found using simulation and a linear regression analysis.

TABLE 3.2

Simulation results of parameter values across process corners

Process Corners	Parameters and Relative Variation					
	$R (\Omega)$	$\Delta R/R$	$K_{pn} (\mu A/V^2)$	$\Delta K_{pn}/K_{pn}$	$V_{TN} (V)$	$\Delta V_{TN}/V_{TN}$
Typical	741	0	430	0	0.164	0
Best	823	11%	457	6.3%	0.138	-15.9%
Worst	659	-11%	421	-2.1%	0.204	24.4%

In Table 3.3 we compare results predicted using sensitivity analysis with the simulated results for three corners for the “initial” and “improved” analog multiplier. The “Typical” corner is when nominal FET and resistor parameter values in the models are used. We defined the “Best” corner as the process corner that yielded the largest differential current (and consequently the highest operating speed) when the “initial” multiplier design was used. The “Worst” case corner is when parameters are chosen that yield a significant decrease in differential current (and consequently the lowest operating speed

One can see in Table 3.3 that as predicted, the use of the “improved” multiplier design resulted in much less variation in the differential current. The agreement between the results predicted by the analysis and by the simulator is good but not perfect. This is not surprising and merely confirms the fact that parameters other than those explicit in the sensitivity analysis contribute to variations in the differential current. It is interesting to note that the variations in the differential current are actually smaller than what was predicted by the analysis. Clearly, the variations observed when the “improved” design is used are about one order of magnitude smaller than when the “initial” design is employed.

TABLE 3.3

Estimated and simulated results in initial and improved multipliers

Process Corners	Initial analog multiplier			Improved analog multiplier		
	$\frac{\Delta I_{out_est}}{I_{out_est}}$	<i>Peak-Peak</i> $I_{out_sim} (\mu A)$	$\frac{\Delta I_{out_sim}}{I_{out_sim}}$	$\frac{\Delta I_{out_est}}{I_{out_est}}$	<i>Peak-Peat</i> $I_{out_sim} (mA)$	$\frac{\Delta I_{out_sim}}{I_{out_sim}}$
Typical	0	391	0	0	720	0
Best	54%	491	26%	-6.5%	724	0.5%
Worst	-48%	167	-57%	17.6%	698	-3.1%

Mismatch and Offset Analysis

It is important that random offsets due to mismatch in transistor parameters t be considered. Clearly, a differential offset current, resulting from mismatches, delivered to the NMOS latch in the comparator of Fig. 2.7 will result in the clock's duty cycle differing from the ideal fifty percent. In fact, if the offset current becomes larger than the peak differential output current, the clock becomes stuck at one logic level. If the duty cycle is to be in the acceptable range of 40 – 60 percent, then the differential offset current must be less than 25% of the differential output current's peak amplitude. In other words, based on the value in Table I, the differential offset current should not exceed 190 μA .

In equation (2.3) the transistor parameters V_{TN} , K_{pn} , W_n , and L_n should be treated as independent Gaussian random variables. It is easy to show that when sensitivity techniques are applied to (2.3), the current predicted by (2.3) will be Gaussian distributed, with mean value, I_{DS} , and the variance given by

$$\sigma_{I_{DS1}}^2 = g_{m1}^2 \cdot \sigma_{V_{TN}}^2 + I_{DS1}^2 \cdot \left(\frac{\sigma_{K_{pn}}^2}{K_{pn}^2} + \frac{\sigma_{W_n}^2}{W_n^2} + \frac{\sigma_{L_n}^2}{L_n^2} \right) \quad (3.4)$$

where the σ^2 are variances associated with the respective variables, g_m is the small-signal transconductance of the NFET, and I_{DS} is the mean DC drain-to-source current. The subscript I highlights the association of the variables with the first-stage combiner.

For the first-stage combiner in Fig. 2.4, the variance of the output voltage may then be written as

$$\sigma_{V_{O1}}^2 = 2R_{eq}^2 \sigma_{I_{DS1}}^2 + (2I_{DS1})^2 \sigma_{R_{eq}}^2 \quad (3.5)$$

where $\sigma_{R_{eq}}^2$ is the variance associated with the resistance, R_{eq} , implemented by the resistive PFET, M_3 . Using the equation (2.10) and a similar sensitivity technique, one may write

$$\sigma_{R_{eq}}^2 = R^2 \cdot \left(\frac{\sigma_{V_{TP}}^2}{V_{SAT}^2} + \frac{\sigma_{K_{pp}}^2}{K_{pp}^2} + \frac{\sigma_{W_p}^2}{W_p^2} + \frac{\sigma_{L_p}^2}{L_p^2} \right) \quad (3.6)$$

where V_{SAT} is the saturation voltage of the PFET M_3 , $\sigma_{V_{TP}}^2$ is the variance of the threshold voltage of M_3 , and $\sigma_{K_{pp}}^2$ is the variance of the transconductance parameter for the PFET. Applying an equation similar to equation (3.4) to the second stage combiners, the variance of the differential offset current can be written as

$$\sigma_{I_{out}}^2 = 8 \cdot g_{m2}^2 \cdot (\sigma_{V_{TN}}^2 + \sigma_{V_{O1}}^2) + 8 \cdot I_{DS2}^2 \cdot \left(\frac{\sigma_{K_{pn}}^2}{K_{pn}^2} + \frac{\sigma_{W_n}^2}{W_n^2} + \frac{\sigma_{L_n}^2}{L_n^2} \right) \quad (3.7)$$

As before the subscript 2 is used to make explicit the variable's association with the second-stage combiner. The factor of 8 is present in equation (3.7) because there are a total of 8 FETS in the second-stage combiners that comprise the two multipliers illustrated in Fig. 2.1.

The standard deviation in threshold voltage is computed using the standard threshold matching equation below

$$\sigma_{V_T} = \frac{1}{\sqrt{2}} \cdot \frac{M_{V_{TA}}}{\sqrt{A_{FET}}} \quad (3.8)$$

where $M_{V_{TA}}$ is an empirically determined (foundry supplied) matching coefficient, and A_{FET} is the gate area of the device under consideration. Similarly, the standard deviation in transconductance parameter is computed using the equation as follow

$$\sigma_{K_p} = \frac{1}{\sqrt{2}} \cdot \frac{M_{K_{pA}}}{\sqrt{A_{FET}}} \cdot K_p \quad (3.9)$$

where $M_{K_{pA}}$ is the matching coefficient for the transconductance parameter. In both instances, matching is improved as gate area is increased.

Device Sizing

Based on considerations associated with the aforementioned effects, appropriate device dimensions were selected for the three transistors comprising the combiner. The use of very short transistor lengths was avoided because (through simulation) it was observed

that device threshold voltages increased significantly as the channel length decreased. We attribute this to “reverse short channel effects”. Halo implants (most likely used in the 90 nm process under consideration) increase the average doping concentration in the channel so that the threshold voltage increases significantly if minimal lengths are used. Increasing the length of a FET also reduces λ . Moreover, increased gate area helps reduce the differential offset current.

For simplicity, the NMOS transistors in both first- and second-stage combiners were sized identically. The size of the devices used in the combiner (refer to Fig. 2.4) is presented in Table 3.4 where ‘ M ’ is the multiplicity value (number of FETs in parallel).

TABLE 3.4

Combiner FET sizes

	Ref	W (μm)	L (μm)	M
Combiner	M_1	6	1	2
	M_2	6	1	2
	M_3	32	1	2

Recall that device M_3 is the PFET operating in the resistive region which simulates the resistance, R , in the original combiner circuit of Fig. 2.3. The control voltage on the gate of M_3 was chosen to be approximately 300 mV resulting in a saturation voltage in excess of 500 mV. A large width-to-length ratio was needed to realize a resistance of around 700 Ω . A

length of 1 μm was chosen in order to improve matching of the pseudo-resistors in the first-stage combiners of the multiplier. In the original combiner design, the dimensions of the n+ diffusion resistor, R , were 10 μm by 78 μm . Clearly, a significant area savings was achieved by adopting the pseudo-resistor in the multiplier design.

The results of the offset analysis from the previous section were used to calculate the expected differential offset current from the two multipliers. We possessed the necessary foundry data needed to compute the variances defined in the previous section. The standard deviation of the offset current, $\sigma_{I_{OUT}}$, was computed as 15 μA . The 6σ value (90 μA) is well below the upper limit of 190 μA which was needed to ensure a reasonable duty cycle for the output clock.

The widths and lengths of the transistor of the bias circuit (Fig. 2.5) and associated OTA (Fig.2.6) in the “improved” analog multiplier are given in Table 3.5. In order to ensure good matching in the layout, the multiplicity (M) for all FETs is 2. This allows the person performing the layout to inter-digitate the devices to achieve better matching.

The device sizes of the *NAND* gate included in *SR* latch (Fig. 2.8), and *T/H* (Fig 2.9) circuit are listed in Table 3.6. The ratio of the width of the PFET to the width of the NFET in the *NAND* gate is chosen to be 1.5 help equalize the rise- and fall-times. In addition, the shape factors of the FETS in the transmission gate in the *T/H* circuit were chosen to be large (lower ON resistance) so that the overall bandwidth of the clock generator will not be limited.

TABLE 3.5

Bias circuit and OTA FET sizes

	Ref	W (μm)	L (μm)	M
Bias Circuit	M ₁ -M ₂	12	4	2
	M ₃ , M ₆	4.5	4	2
	M ₇ -M ₈	1.3	4	2
	M ₉ -M ₁₀	1.4	4	2
	M ₁₀ , M ₁₁	3.3	0.25	2
	M ₁₇ -M ₁₈	6	1	2
OTA	M ₁₉	32	1	2
	M ₂₀ -M ₂₁	1	2	2

TABLE 3.6

NAND gate and T/H circuit FET sizes

	Ref	W (μm)	L (μm)	M
NAND	M ₁ -M ₂	6	0.2	2
	M ₃ -M ₄	4	0.2	2
T/H	M ₁ , M ₃	6	0.2	2
	M ₂ , M ₄	2	0.2	2
	M ₅	28.8	0.2	2
	M ₆	9.6	0.2	2

The widths and lengths of the transistors in the analog comparator, illustrated in Fig. 2.7, are listed in Table 3.7

TABLE 3.7

Comparator FET sizes

	Ref	W (μm)	L (μm)	M
Comparator	M ₁ , M ₄	1.5	0.25	1
	M ₂ , M ₃	1.5	0.25	2
	M ₅ -M ₈	19.8	0.25	2
	M ₉	15.3	0.25	2
	M ₁₀ , M ₁₁	3.3	0.25	2
	M ₁₂ , M ₁₃	0.95	0.25	2
	M ₁₄	4.2	0.25	2
	M ₁₅	3.00	0.50	1
	M ₁₆	1.00	0.50	1

CHAPTER 4

SIMULATION RESULTS

In this chapter, we report the results of simulations performed on the restartable clock generator and its sub-circuits. Electrical simulations were performed using Cadence's *Spectre*® simulator. The BSIM4 model was used for the FETs. The power supply voltage was 1 Volt. The frequency of the quadrature inputs was 1 GHz and the DC level of the inputs (V_B voltage) was 570 mV. The peak-to-peak amplitude of the input signal was 400 mV. The bias current for the OTA was 10 μ A.

Analog Multiplier Simulation

The differential current output and one of the four quadrature sinusoidal inputs are illustrated in Fig. 4.1. The peak-to-peak amplitude of the current is approximately 700 μ A (See Table 3.3). No obvious distortion is present. The output frequency is 2 GHz, twice the input frequency, which can be easily proved by using equation (2.8).

Frequency Response of Symmetrical Miller OTA

The gain and phase plots for the symmetric Miller OTA are presented in Fig. 4.2. The low frequency open-loop gain is close to 32 dB, the Gain Bandwidth product (GBW) is about 5.7 MHz and the phase margin is 60° approximately ($180^\circ - 120^\circ$). Since the OTA is used to stabilize the DC level only a small GBW is required. The low gain (32 dB) explains why the simulated value for V_{BO1} in Table 3.1 deviates slightly from its expected value. In order to increase the open loop gain a cascode structure could be employed in the OTA design, but this is difficult because of the small supply voltage (1 Volt).

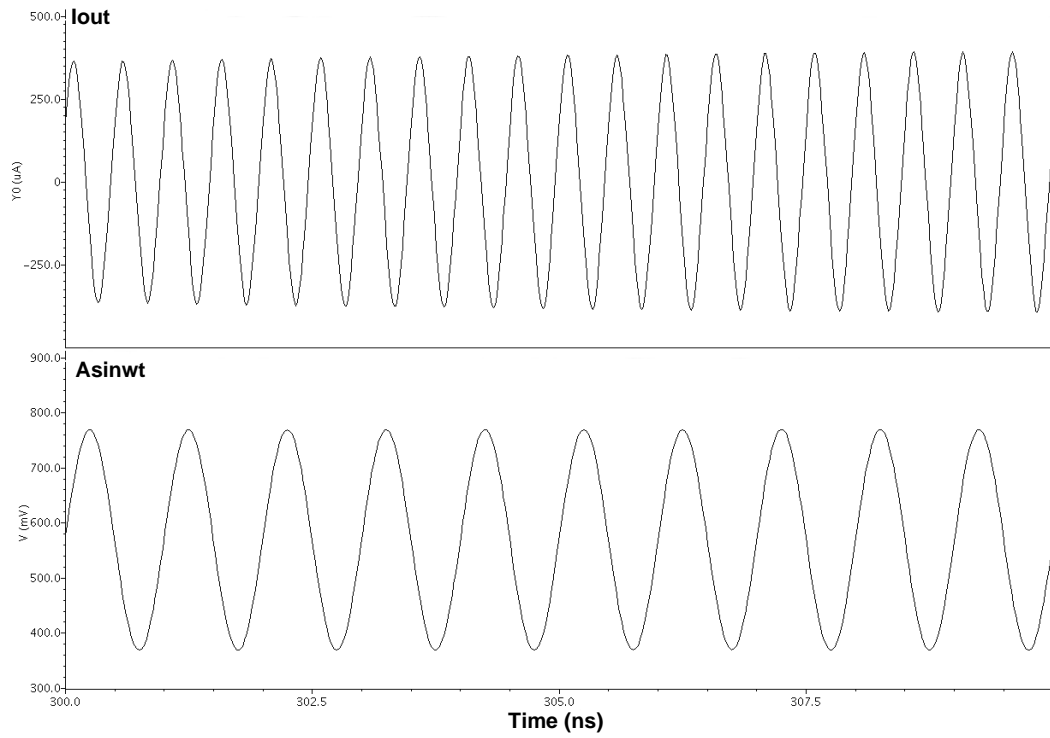


Fig. 4.1 Analog multiplier simulation

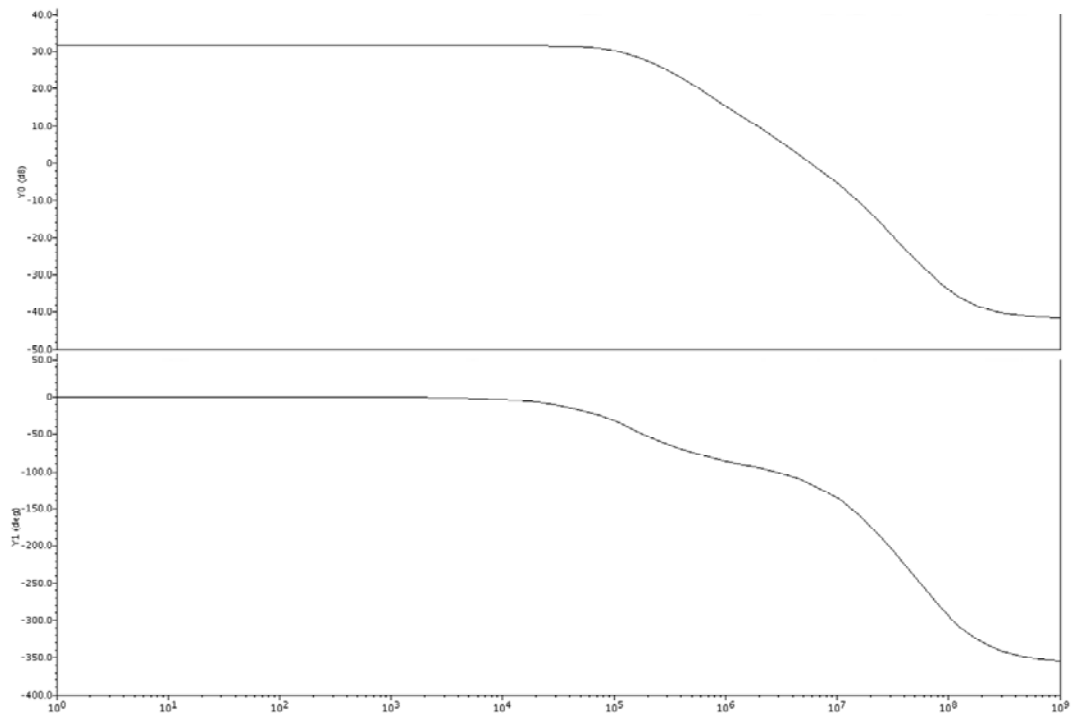


Fig. 4.2 Frequency response of symmetric Miller OTA

Hold Signal Verification

The correctness of the hold signal is verified in simulation, illustrated in Fig. 4.3. When either one of ‘*Init!*’ signals is asserted, the output of the *OR* gate (‘Hold’ signal) goes high and forces the *T/H* circuit into “hold” mode. If the ‘*Done!*’ signal is applied, then both *SR* latches are reset. The ‘Hold’ signal changes to a low level and forces the *T/H* circuit into “track” mode.

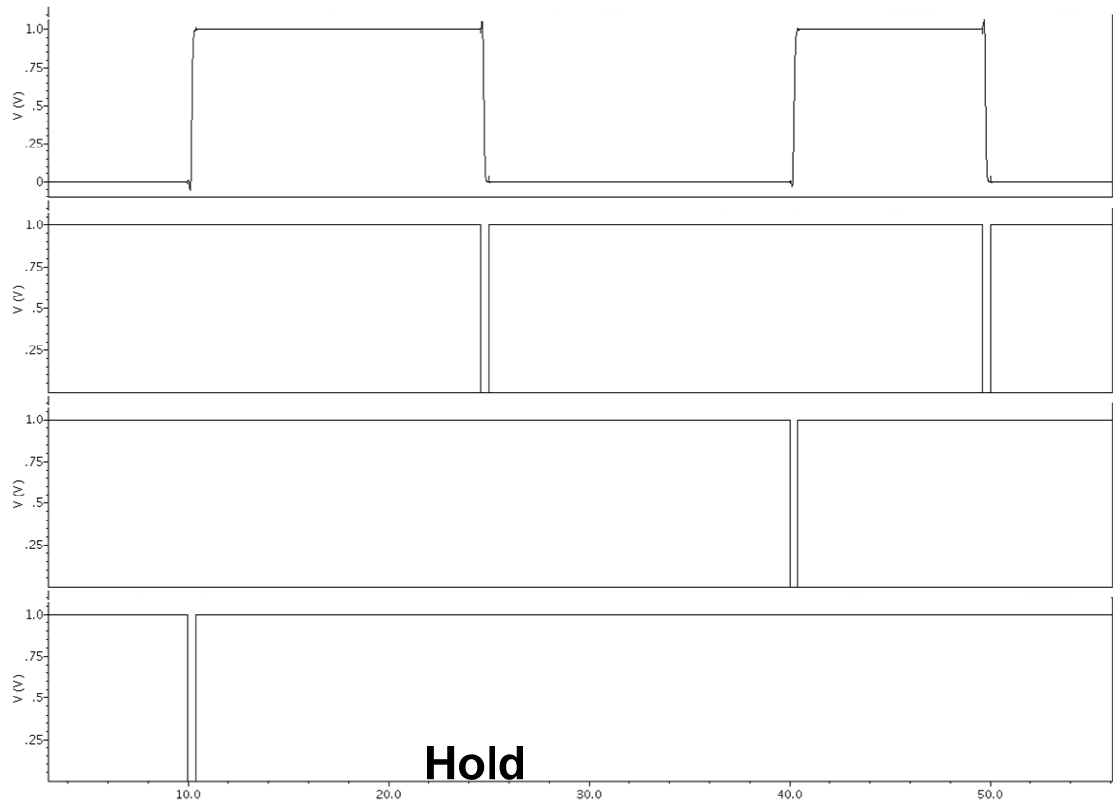


Fig. 4.3 Hold signal verification

Done !

Track and Hold Circuit Simulation

Fig. 4.4 depicts one of the quadrature sinusoidal inputs passing through the T/H circuit. Clearly, the output tracks the input when the ‘Hold’ signal is low. When ‘Hold’ transitions high the analog voltage at the input is held at the output of the T/H . The voltage is changed by a small amount due to “clock feedthrough” and “charge injection” effects [All:03].

The bandwidth of the T/H circuit also has been simulated and is shown in Fig. 4.5. The -3dB bandwidth is 3.2 GHz. This value is large enough so as not to degrade the overall bandwidth of the clock generator.

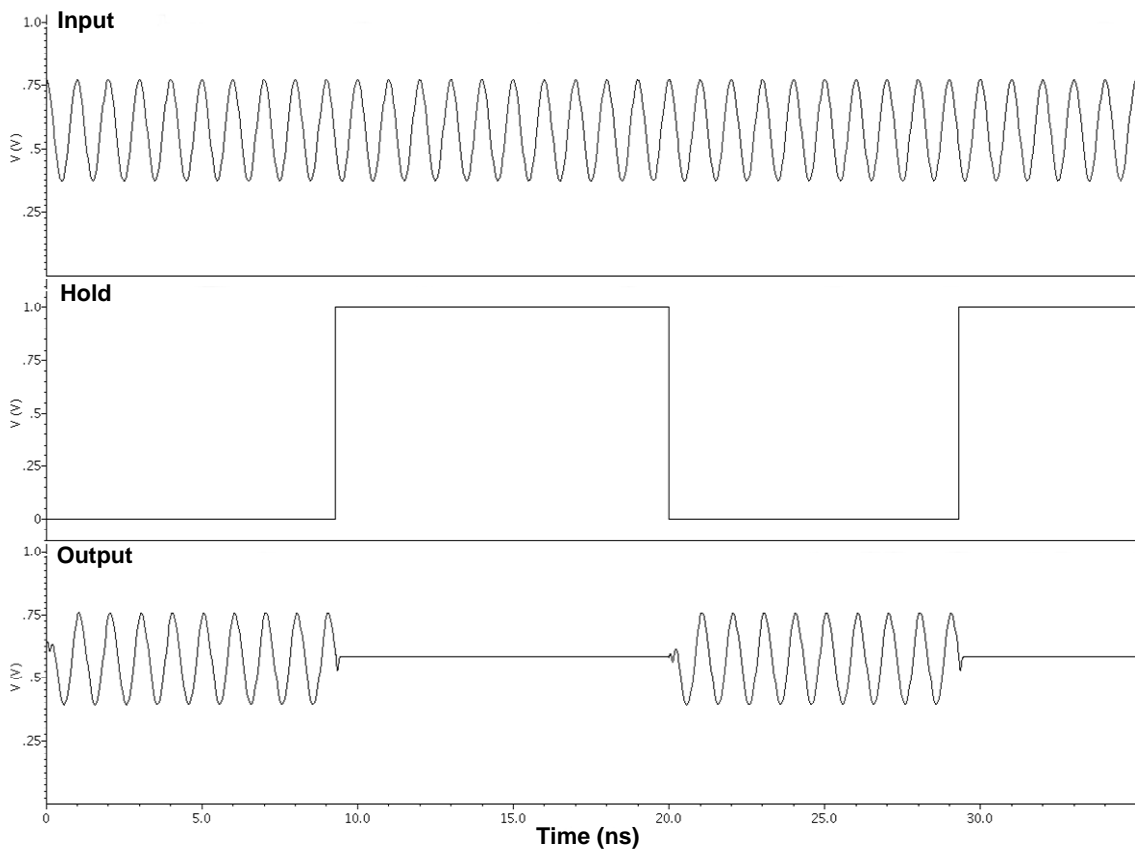


Fig. 4.4 Transient response of T/H circuit

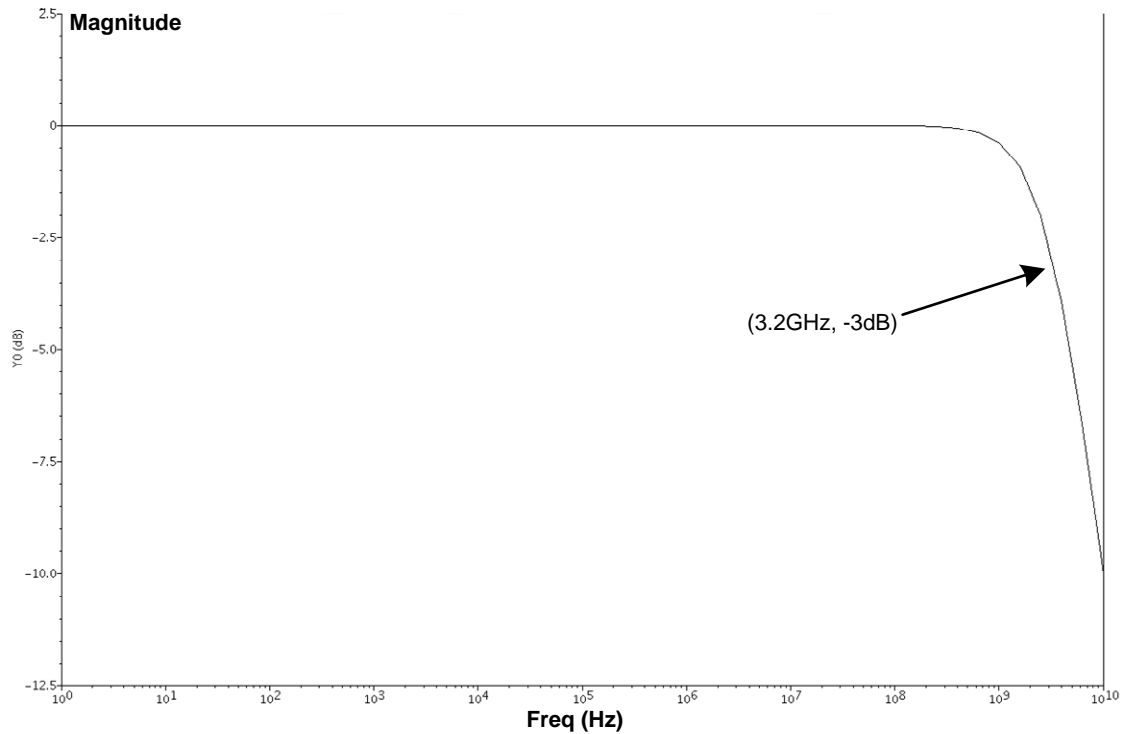


Fig. 4.5 Frequency response of T/H circuit

Restartable Clock Generator Simulation

Correct operation of the clock generator is illustrated in Fig. 4.6. The sine wave input in the figure is one of the four quadrature inputs applied to the multiplier. The square wave output, which serves as the clock to a data processing subsystem in our blended design methodology, is started whenever the ‘*Init!*’ signal is pulsed low and is stopped when the ‘*Done!*’ signal is pulsed low. It is restarted with the next ‘*Init!*’ signal. The duty cycle of the clock is near 50% which is expected since no random offsets which would alter the duty cycle were modeled in the simulation.

As described in Chapter 3 since the multiplier is fully differential, its linearity is inherently quite good. In Fig. 4.6, I_{out} is the differential current delivered to the NMOS latch

in the comparator. Note the absence of any significant distortion in this differential current waveform. Moreover, the waveforms in the figure change very little as the process corner is changed because of the technique which we used to stabilize the gain of the multipliers.

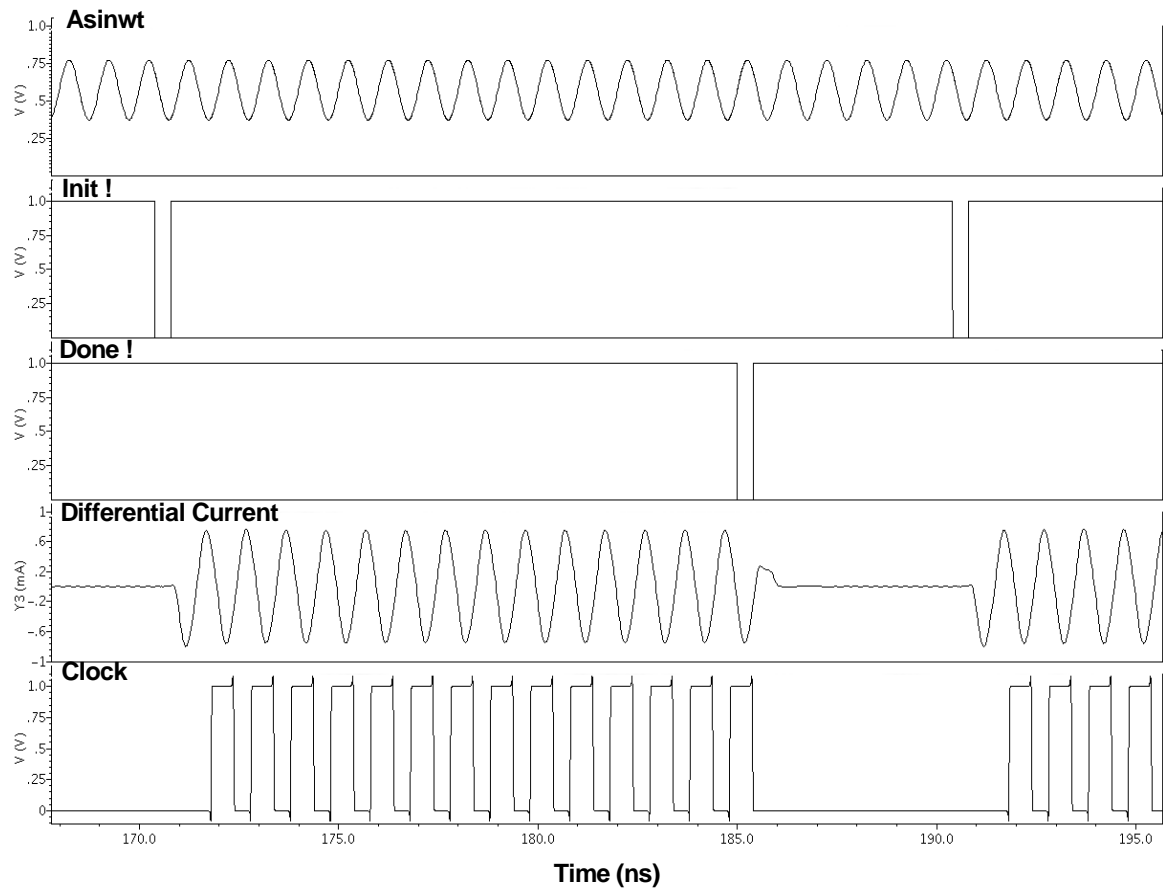


Fig 4.6 Clock generator simulation

In Fig. 4.7 the delay in starting the clock, measured from the falling edge of the ‘*Init!*’ signal to the rising edge of the output clock, is plotted. The graph is generated by uniformly distributing the arrival of the ‘*Init!*’ signal over one period of the reference input sinusoid. One can see from the figure that the average delay in restarting the clock is approximately 1.5 ns. This value includes the delay inserted by the *SR* latch, the *OR* gate, track and hold circuits, analog multipliers, and the comparator. The peak-to-peak variation in the time required to restart the clock is 120 *psec*.

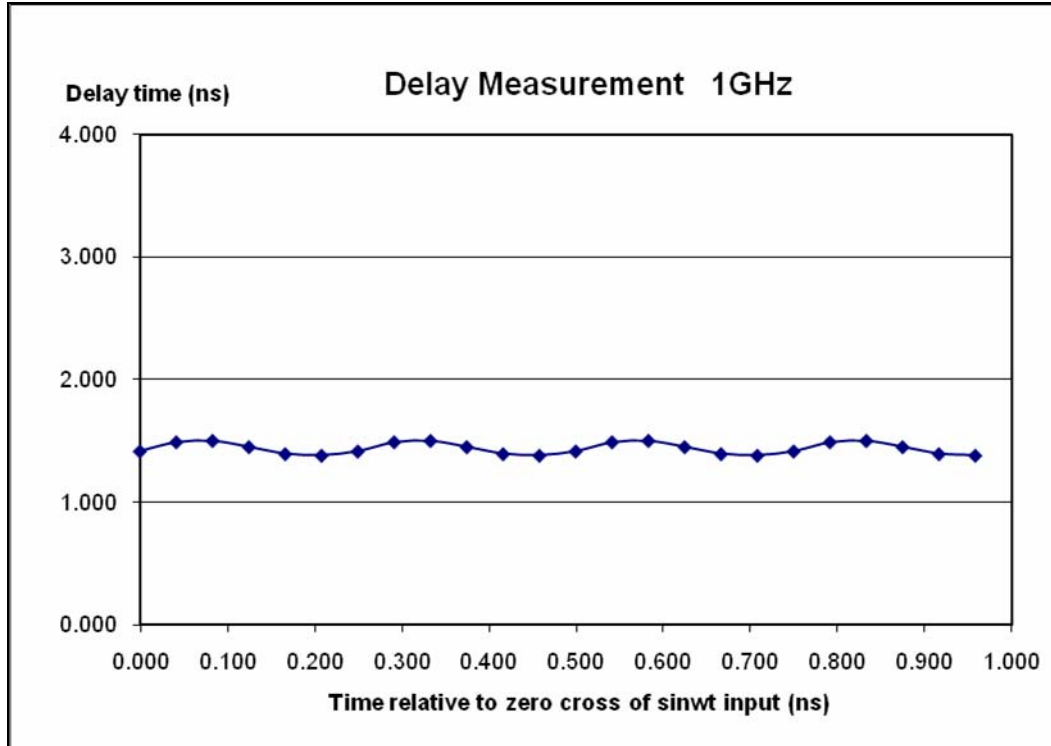


Fig. 4.7 Delay associated with restarting the clock

CHAPTER 5

CONCLUSIONS AND FUTURE WORK

Conclusions

Synchronizers are the accepted method for communication between clockless and clocked domains, but they present metastability hazards [Cha:73]. These hazards can be effectively mitigated, but not eliminated by proper synchronizer design [Stu:79]. However, each such design is unique to a specific IC process. A new design presented in this thesis, the “restartable” clock, is based on a fixed-period source eliminating the variation in periodicity, characteristic of pausable clocks presented in the literature. However, like a delay-based clock the restartable clock can be stopped and then restarted at an arbitrary phase of the source.

This restartable clock completely eliminates metastability hazards and can be scaled with feature size across IC processes without introducing metastability. The proposed restartable clock can be based on an external crystal oscillator or on a local all-silicon, MEMS-based oscillator. The later approach has the advantage of eliminating global clock trees and their dissipation, suppressing clock noise, and reducing power consumption during subsystem idle time.

Furthermore, the thesis demonstrates that it is possible to design a plausible clock based on an external crystal oscillator or MEMS-based oscillator that is fully compatible with modern deep sub-micron technologies. The circuit described here, implemented in a state-of-the-art 90 nm process, only makes use of regular threshold voltage FETS, operates from a single 1 Volt power supply, and is insensitive to process variations, In addition the clock generator circuit exhibits low power dissipation while able to operate at frequencies as high

as 1 GHz and with a latency of 1.5 clock periods. Higher frequency operation is possible but at the expense of both power dissipation and area.

Future Work

Monte Carlo simulations to confirm the results presented in Chapter 4 predicting the likely offset current will be performed in the future. Also, the clock generator requires quadrature signals, the generation of which was not addressed in this thesis. Future work will tackle the task of efficiently generating these signals from an external crystal oscillator or MEMS-based clock.

REFERENCES

- [All:03] Phillip E. Allen, Douglas R. Holberg, *CMOS Analog Circuit Design (2nd Ed.)*, Oxford University Press, pp. 477-487, 2003.
- [Ami:07] Esmail Amini, Mehrdad Najibi and Hossein Pedram, “*FPGA Implementation of Gated Clock Based Globally Asynchronous Locally Synchronous Wrapper Circuits*” 2007
- [Bai:03] W. J. Bainbridge, W. B. Toms, D. A. Edwards, S. B. Furber, “Delay-Insensitive, Point-to-Point Interconnect using m-of-n Codes,” *Proceedings of the Ninth International Symposium on Asynchronous Circuits and Systems (ASYNC.03)*, pp 132-140, May 2003.
- [Bei:08] E.Beigné, F. Clemidy, S. Miermont, and P. Vivet, *Dynamic Voltage and Frequency Scaling Architecture for Unit Integration within a GALS NoC*, In proc Second ACM/IEEE International Symposium on Networks-on-Chip, page 129-138, Apr.2008
- [Cha:73] T. J. Chaney, C. E. Molnar, “*Anomalous behavior of synchronizer and arbiter circuits,*” *IEEE Trans. on Computers*, C-22, pp.421-422, 1973.
- [Cha:84] D.M. Chapiro, “*Globally-Asynchronous Locally-Synchronous Systems*”, Ph.D. thesis, Stanford University, Oct. 1984.
- [Cla:67] W. A. Clark “*Macromodular computer systems,*” *Spring Joint Computer Conf., AFIPS Proceedings*, 30, Thompson Books, Washington D.C., pp. 335-336, 1967.
- [Cla:74] W. A. Clark, C. E. Molnar, “*Macromodular computer systems,*” *Computers in Biomedical Research*, 4, R. Stacy and B. Waxman, Eds. Academic Press, New York, pp 45- 85, 1974.
- [Cox:88] J.R. Cox, “*Can a crystal clock be started and stopped?*” *Applied Mathematics Letters*, Vol. 1, Pergamon, pp 37-40, 1988.
- [Cox:05] J. R. Cox and D. M. Zar, “*Blending clockless and clocked subsystems using macromodular control elements,*” *WU CSE Tech. Report*, 2005-43.
- [Cox:07] J.R. Cox, G.L. Engel, D.M. Zar “*Design of Instantaneously Restartable Clocks And Their Use Such As In Connecting Clocked Subsystems Using Clockless Sequencing Networks*”, United States Patent #7,243,255; July 10, 2007.

- [Deb:02] Carl James Debono, Franco Maloberti, and Joseph Micallef, “*On the Design of Low-Voltage, Low-Power CMOS Analog Multipliers for RF Applications*”, IEEE Trans. Very Large Scale Integr., Vol. 10, No. 2, pp 168-174, April 2002.
- [Dob:99] Rostislaav Dobkin, Ran Ginosar, and Christos P. Sotiriou, “*High Rate Data Synchronization in GALS SoCs*”, IEEE Trans. Very Large Scale Integr., Vol. 14, No. 101, pp. 1063-1074, December 1999.
- [Gür:06] Frank K. Gürkaynak, Stephan Oetiker, Hunbert Kaeslin, Norbert Felber, and Wolfgang Fichtner, “*GALS at ETH Zurich: Success or Failure?*” In Proc. International Symposium on Advanced Research in Asynchronous Circuit and Systems, page 150-159 Mar. 2006
- [Hsi:98] S.-Y. Hsiao and C.-Y. Wu, “*A parallel structure for CMOS four-quadrant analog multipliers and its application to a 2-GHz RF downconversion mixer*,” IEEE J. Solid-State Circuits, vol. 33, pp. 859-869, June 1998.
- [Lak:94] Kenneth R. Laker and Willy M. C. Sansen, *Design of Analog Integrated Circuits and Systems*, McGraw-Hill Press, pp 219-221, 1994.
- [Mob] Mobius Microsystems: web site: <http://www.mobiusmicro.com>
- [Sei:80] C. L. Seitz, “System timing,” In: C. A. Mead, L. A. Conway, Eds, *Introduction to VLSI systems*, Chapter 7, Addison-Wesley, 1980.
- [Stu:79] M. J. Stucki and J. R. Cox, “Synchronization strategies,” *Proceedings of Caltech Conference on VLSI*, pp. 375-393, Jan. 1979.
- [Tal:05] S.K. Tallapragada, “*Design of a Restartable Crystal Controlled Clock for Use in a Globally Asynchronous, Locally Synchronous Design Methodology*” Master Project Report, Southern Illinois University Edwardsville, December 2005.
- [Tra:91] Cherrice A. Traver, “*A Testable Model for Stoppable Clock ASICs*”, ASIC Conference and Exhibit, 1991. Proceedings., Fourth Annual IEEE International, pages 6-3/1-5, Sept. 1991
- [Ung:69] Stephen Unger, *Asynchronous sequential switching circuits*, Wiley-Interscience, pp. 177-183, 1969.
- [Yun:99] Kenneth Y. Yun and Ayoob E. Dooply, “*Pausable Clocking-Based Heterogeneous Systems*”, IEEE Trans. Very Large Scale Integr., Vol. 7, No. 4, pp 482-488, December 1999.